1 **Aerosol light absorption and the role of extremely low volatility organic**

2 **compounds**

4 Antonios Tasoglou[1,5], Evangelos Louvaris[2,3], Kalliopi Florou[2,3] Aikaterini Liangou[2,3], Eleni

5 Karnezi[1] Christos Kaltsonoudis[4], Ningxin Wang[1], Spyros N. Pandis[1,2,3]

6 [1]Department of Chemical Engineering, Carnegie Mellon University, Pittsburgh
7 [2]Department of Chemical Engineering, University of Patras, Patras, Greece
8 [3] Institute of Chemical Engineering Sciences (ICE-HT), FORTH, Patras, Greece
9 [4]Department of Mechanical Engineering, Carnegie Mellon University, Pittsburgh, United States
10 [5]RJ Lee Group, Inc., Monroeville, United States

12 **Abstract**

13   A month-long set of summertime measurements in a remote area in the Mediterranean is

14 used to quantify aerosol absorption and the role of black and brown carbon. The suite of

15 instruments included a high-resolution Aerosol Mass Spectrometer (HR-ToF-AMS), and a

16 Scanning Mobility Particle Sizer (SMPS) both coupled to a thermodenuder and an aethalometer,

17 a photoacoustic extinctiometer (PAX$_{405}$), a Multi-Angle Absorption Photometer (MAAP), and a

18 Single Particle Soot Photometer (SP2).

19   The average refractory black carbon (rBC) concentration during the campaign was 0.14 μg

20 m^{-3}, representing 3% of the fine aerosol mass. The measured light absorption was two or more

21 times higher than that of fresh black carbon (BC). Mie theory indicated that the absorption

22 enhancement due to the coating of BC cores by non-refractory material could explain only part of

23 this absorption enhancement. The role of brown carbon (BrC) and other non-BC light-absorbing

24 material was then investigated. A good correlation (R^2=0.65) between the unexplained absorption

25 and the concentration of extremely low volatility organic compounds (ELVOCs) mass was found.

26

27 **1. Introduction**

28   Atmospheric aerosol may influence climate in two ways: directly through scattering and

29 absorbing radiation, and indirectly through acting as cloud condensation nuclei (IPCC, 2011)

30 Black carbon is the dominant light absorbing aerosol component. BC is a distinct type of

31 carbonaceous material that is formed mainly during combustion processes. In addition, some

32   organic aerosol (OA) has the ability to absorb sunlight. The OA with strong light absorption is

33   called brown carbon (BrC) (Andreae et al., 2006).

34   The absorption of BC depends on its mixing state (Liu et al., 2015, 2017). Usually, BC is

35   coated with scattering material causing its light absorption to increase due to the lensing effect

36   (Fuller et al., 1999; Jacobson, 2001; Bond et al., 2006; Lack and Cappa, 2010). The absorption

37   enhancement (E_{abs}) is defined as the ratio of the aerosol absorption coefficient (b_{abs}) over the b_{abs}

38   of the pure BC particles. This enhancement can also be calculated by the ratio of the equivalent

39   mass absorption cross-sections (MAC). The MAC is defined as the ratio of b_{abs} over the BC mass.

40   The E_{abs} can be measured by using a thermodenuder (TD) for the removal of the non-refractory

41   coating material from the BC containing particle, or it can be estimated using a theoretical model

42   (for example Mie or Rayleigh-Debye-Gans theory) if the particle morphology is known.

43   Incomplete removal of the non-refractory material in the TD can lead to underestimation of the

44   E_{abs} (Healy et al., 2015; McMeeking et al., 2014).

45   Previous studies have demonstrated that lensing has a strong effect on the light absorption

46   of BC. Liu et al. (2015) found a campaign average E_{abs} of 1.3 at wavelength (λ) equal to 405 nm

47   and 1.4 at 781 nm in a rural area near London during the winter. They also suggested that the lower

48   volatility BrC has stronger absorption than the semi-volatile BrC. Knox et al. (2009) performed

49   measurements in downtown Toronto, during the wintertime using a TD at 340 °C. They reported

50   an E_{abs} of 1.43 for fresh particles, based on thermal OC/EC and photoacoustic measurements. Liu

51   et al. (2017) combined laboratory experiments with diesel exhaust emissions and ambient

52   measurements to show that particles with a ratio of non-refractory PM to BC mass (R_{BC}) less than

53   1.5 (typical for traffic emissions) had a negligible lensing effect. When the R_{BC} was above 3,

54   lensing caused significant enhancement of the absorption of BC. Zhang et al. (2018a) presented

55   three years of measurements in a suburban cite outside Paris, France, influenced by both fresh and

56   aged air masses. On average they found an E_{abs}=2.07 at 370 nm, and an E_{abs}=1.53 at 880 nm. They

57   calculated the E_{abs} by measuring the absorption coefficient (b_{abs}) with an aethalometer, while the

58   elemental carbon (EC) was measured with thermal methods using daily filters. Zhang et al. (2018b)

59   presented measurements in Beijing, China during wintertime. Using aethalometer measurements,

60   refractory and non-refractory particle size distributions and Mie theory, they calculated that the

61   lensing effect led to an E_{abs} ranging from 1.5 to 2 on average at 880 nm. Zanatta et al. (2018) found

62   an E_{abs}=1.54 at 550 nm for measurements at the Zeppelin Arctic Station. Lack et al. (2012)

63   analyzed measurements of biomass burning plumes near Boulder, CO during summertime. Using

64   a TD at 200 ºC, they found E_{abs} values as large as 2.5 at 404 nm and 1.7 at 532 nm. Using the

65   absorption Angström exponent (AAE) and Mie theory calculations they showed the presence of

66   BrC.

67   Some studies have argued that Mie theory may overestimate the E_{abs}. Cappa et al. (2012)

68   suggested that the absorption enhancement of BC in California in the summertime was low with

69   values equal to 1.13 at 405 nm and 1.06 at 532 nm for R_{BC}>10. For their measurements they used

70   a TD operated at 225 ºC and 250 ºC. Hearly et al. (2015) also reported practically no enhancement

71   in the BC absorption at 781 nm and E_{abs}=1.19 at 405 nm in Toronto, Canada during summertime.

72   During a period associated with wildfires the same authors measured R_{BC}=6.9 and E_{abs}=1.39 at

73   405 nm. They argued that there was little evidence of the lensing effect, and that BrC was driving

74   the E_{abs}. Cappa et al. (2019) performed measurements in Fresno, CA during wintertime and

75   Fontana, CA during summertime. They found that in Fresno there was absorbing OA, BrC, which

76   was related to biomass burning OA and nitrate-associated OA. In Fresno, they reported average

77   E_{abs} of 1.37, 1.22 and 1.1 at wavelengths equal to 405, 532, 781 nm, respectively, for R_{BC} ranging

78   from 1 to 4. In Fontana the E_{abs} was lower with values of 1.1 at 405 nm and 1.07 at 532 nm.

79   Laboratory measurements of McMeeking et al. (2014) for biomass burning aerosol indicated

80   higher absorption in lower wavelengths compared to higher ones and thus the presence of BrC. No

81   enhancement of absorption was observed at R_{BC}<1. On average they found an E_{abs} equal to 1.25 at

82   781 nm with a maximum value of E_{abs}=4 for R_{BC}>10.

83   Recent studies have suggested that the absorption efficiency of OA could be related to its

84   volatility. Saleh et al. (2014) in their laboratory biomass burning experiments showed that almost

85   all absorbing OA was associated with extremely low volatility compounds (ELVOCs), with an

86   effective saturation concentration C^* of 10^{-4} µg m^{-3}. In addition, Saleh et al. (2018) using controlled

87   combustion experiments showed that the absorption activity of BrC is proportional to its molecular

88   size.

89   Despite the significant progress in understanding the absorption of atmospheric fine aerosol

90   there are still remaining questions regarding both the absorption enhancement of black carbon and

91   the absorption of OA as the aerosol evolves in the atmosphere. In this study we try to address these

92   issues for aerosol that has been aged in the atmosphere for at least a few days before arriving at

93   the island of Crete in the Eastern Mediterranean.

2. Experimental Methods

A remote location in the Eastern Mediterranean was used for the study of the absorption and volatility of aged carbonaceous aerosol. The area is characterized by intense photochemistry, especially during the summer (Pikridas et al., 2010) and is affected by pollutants transferred from continental Europe, Turkey, Greece and Africa (Mihalopoulos et al., 1997; Lelieveld et al., 2002; Kalivitis et al., 2011; Bougiatioti et al., 2014). Previous measurements have shown that the OA reaching the area is highly oxidized regardless of its origin (Hidlebrandt et al., 2010; 2011). Lee et al. (2010) showed that these oxidized organic compounds have much lower volatility than fresh SOA. Long-term measurements in the region have revealed relatively high light absorption and scattering by aerosol during the summer (Kalivitis et al., 2011; Vrekoussis et al., 2005).

The FAME-16 field campaign took place from May 9 to June 2, 2016. Measurements were conducted at the Finokalia Station (*35° 20′ N, 25° 40′ E*, 250 m asl), a remote site on the island of Crete in Greece (Mihalopoulos et al., 1997). The nearest large city is Heraklion with 150,000 inhabitants located 50 km west of Finokalia (Kouvarakis et al., 2000). There are no local sources near the station, allowing the investigation of aged OA from different source regions. During this study, two Saharan dust events occurred from May 12 till May 15 and May 21 till May 22.

A Scanning Mobility Particle Sizer (SMPS, TSI classifier model 3080, CPC model 3775) was used to measure the number and the size distribution of the particles. The aerosol flow was set at 1 L min^{-1} and the sheath flow at 5 L min^{-1}. The sampling time was 3 min.

The mass concentration and the chemical composition of the particles were monitored using a High-Resolution Time-of-Flight Aerosol Mass Spectrometer (HR-ToF-AMS, Aerodyne Research, Inc.). SQUIRREL 1.56D and PIKA v1.15D were used for the data analysis, while for the elemental ratio calculations the improved ambient calculation approach of Canagaratna et al. (2015) was used. The HR-ToF-AMS was operated in V-mode with a sample time of 3 min. The collection efficiency of the HR-ToF-AMS was calculated using the algorithm of Kostenidou et al. (2007). The average CE was 0.64±0.2. Positive matrix factorization (PMF) analysis (Lanz et al., 2007; Paatero and Tapper, 1994; Ulbrich et al., 2009) was performed using as input the high resolution OA mass spectra and the mass-to-charge ratios (*m/z*) from 12 to 200.

A Single Particle Soot Photometer (SP2, Droplet Measurement Technologies) was used to measure the BC. The instrument was calibrated using fullerene soot (Alfa Aesar, stock 40971, lot L20W054) (Gysel et al., 2011). The calibration of the SP2 was verified in separate experiments

125   using a centrifugal particle mass analyzer (CPMA, Cambustion) (Saliba et al., 2016). The data

126   were analyzed using the Probe Analysis Package for Igor. In our measurements, the number

127   concentration of BC was low (<10,000 particles cm^{-3}), and thus it was assumed that there were no

128   coincidence artifacts in our measurements. The scattering measurement was calibrated using

129   monodisperse polystyrene latex (PSL) spheres.

130   A photoacoustic extinctiometer (PAX, Droplet Measurement Techniques) with a blue (405

131   nm) laser was used to measure the absorption (b_{abs}) and the scattering (b_{scat}) coefficients. Fullerene

132   soot and PSL spheres were used to calibrate the absorption and scattering signals, respectively. An

133   activated carbon denuder was placed in front of the PAX to remove NO_2. Furthermore, a seven

134   wavelength aethalometer (AE31, Magee Scientific) was used to measure the b_{abs} at 370, 470, 520,

135   590, 660, 880 and 950 nm and to calculate the absorption Angstrom exponent (AAE), which

136   describes the wavelength dependence of the b_{abs}. The aethalometer measurements were corrected

137   for scattering and multiple scattering artifacts following Saleh et al. (2014) and Tasoglou et al.

138   (2017) using the corrections suggested by Weingartner et al. (2003) and Kirchstetter and Novakov

139   (2007).

140   The thermodenuder (TD) used in this study, was placed upstream of the HR-ToF-AMS and

141   the SMPS. The TD design was similar to that developed by An et al. (2007) and is described by

142   Louvaris et al. (2017). The TD was operated at temperatures ranging from 25 °C to 400 °C using

143   several temperature steps. One complete cycle from 25 to 400 °C and back to 25 °C lasted

144   approximately 10 h. Sampling was alternated between the ambient line and the TD line every 3

145   minutes using computer-controlled valves. Changes in particle mass concentration, composition,

146   and size due to evaporation in the TD were measured by the HR-ToF-AMS and the SMPS resulting

147   in thermograms of OA mass fraction remaining (MFR) as a function of TD temperature. The OA

148   MFR was calculated as the ratio of organic mass concentration of a sample passing through the

149   TD at time t_i over the average mass concentration of the ambient samples that passed through the

150   bypass line at times t_{i-1} and t_{i+1}. The sample residence time in the centerline of the TD was 14 s at

151   25 °C, corresponding to an average residence time in the TD of 28 s. The MFR values were

152   corrected for particle losses in the TD due to diffusion and thermophoresis. To account for these

153   losses, sample flow rate as well as size- and temperature-dependent loss corrections were applied

154   following Louvaris et al. (2017) corresponding to the operating conditions during the campaign.

155   The final step of the data analysis was to average the corrected for CE and TD losses MFR data

156   based on temperature bins of 10°C. The MFR calculation assumes implicitly that the OA

157   concentration remains constant during the measurement period. To ensure that this condition is

158   satisfied, if two consecutive OA ambient mass concentrations differed by more than 25%, the

159   corresponding MFR was not included in the analysis. Also, in order to ensure that the temperature

160   was constant during the measurement, the absolute difference between the two samples had to be

161   less than 5°C. If this difference for a TD sample was higher, then the sample was not included in

162   our analysis. The same approach was used also for the factors resulting from the PMF analysis of

163   the AMS spectra. However, in this case a minimum concentration threshold of 0.1 $\mu g\ m^{-3}$ was used

164   for the ambient concentrations together with the criterion of the stability of the ambient

165   concentrations during the sampling period. MFR values corresponding to concentrations of the

166   PMF factors below this threshold were not included in the dataset. Approximately 75% of the OA

167   samples satisfied all these constraints and were used in the analysis. The corresponding

168   percentages were 65% and 70% for the two identified PMF factors. In the present work the

169   complete datasets will be analyzed together, averaging the corresponding measurements. More

170   details regarding the data analysis and the sensitivity tests of the TD measurements are provided

171   in the supplementary information.

172   The concentrations of gas-phase pollutants were measured using a Proton-Transfer

173   Reaction Mass Spectrometer (PTR-QMS 500, Ionicon Analytik) and gas monitors. The PTR-MS

174   was calibrated with a standard gas mixture of VOCs. The concentration of O_3 was measured using

175   a continuous O_3 analyzer (Thermo Scientific, 49i) and the concentrations of nitrogen oxides were

176   measured using a $NO/NO_2/NO_x$ analyzer (Thermo Scientific, 42i-TL).

177

178   **3. Theoretical Analysis Methods**

179   The dynamic TD evaporation model of Riipinen et al. (2010) together with the uncertainty

180   estimation algorithm of Karnezi et al. (2014) were used for the determination of the OA volatility

181   distribution. Inputs for the model included the ambient OA concentration, the OA density

182   calculated by the algorithm proposed by Kostenidou et al. (2007), the initial average particle size,

183   TD temperature, the MFR values, and TD residence time. In the volatility basis set framework of

184   Donahue et al. (2006), the volatility distribution is represented with a range of logarithmically

185   spaced C^* bins along a volatility axis. In this study 6 bins with variable mass fractions were chosen.

186   For this 6-bin solution, the best 2% of the mass fraction combinations with the lowest error were

187   used to estimate the average mass fraction along with their corresponding standard deviation for

188   the uncertainty of each bin. Additionally the parameters that affect indirectly the calculated

189   volatility such as the effective vaporization enthalpy (ΔH_{vap}), and the effective accommodation

190   coefficient (a_m) were estimated following Karnezi et al. (2014). Additional information regarding

191   the data analysis of the TD measurements are in the supplemental information (sections S1 and

192   S2).

193   A Mie theory model based on the work of Bohren and Huffman (1983) was used to

194   calculate the theoretical MAC and E_{abs}. Mie theory describes the extinction of light by spherical

195   particles due to an incoming planar electromagnetic wave. The calculations were based on the

196   SMPS and SP2 size distributions. For the BC core we assumed a refractive index of the core

197   n_{rBC}=1.85+0.71i (Bond and Bergstrom, 2006) and a density of 1.8 g cm^{-3} (Mullins and Williams,

198   1987; Park et al., 2004; Wu et al., 1997). A non-absorbing coating of the BC core was assumed,

199   with a refractive index of n_{OA} = 1.55 (Bond and Bergstrom, 2006). The total aerosol effective

200   density used was calculated based on the SMPS and HR-ToF-AMS distributions. The average

201   effective density for the campaign was 1.66±0.11 g cm^{-3}. The other inputs of the model were the

202   measured BC size distributions from the SP2 and the ratio of the total aerosol mass over the BC

203   mass as measured by the SMPS and the SP2, respectively.

204

205   **4. Results and discussion**

206   The average rBC concentration of the campaign was 0.14 μg m^{-3} and the average OA

207   concentration was 1.5 μg m^{-3} (Figure 1). The two major Saharan dust events affected, as expected,

208   the aerosol optical properties. In the present study we focus only on the non-dust periods. The

209   dominant PM$_1$ components were sulfate and OA, accounting for 46% and 34% of the PM$_1$,

210   respectively. The O:C ranged from 0.65 to 1, with an average value of 0.83. These values are

211   typical in Finokalia during the spring and summer periods (Hidlebrandt et al., 2010).

212

213   **4.1 OA Volatility**

214   The estimated volatility distribution for the total OA in Finokalia during FAME-16 is

215   depicted in Figure 2. Use of OA with $C^* = 10^{-8}$ μg m^{-3} was needed to capture the behavior of the

216   OA at 400 °C. Almost 40% of the OA consisted of semi-volatile organic compounds (SVOCs),

217 35% of low volatility organic compounds (LVOCs), and the rest was extremely low volatility

218 organic compounds (ELVOCs).

219   The estimated value of the effective vaporization enthalpy was $80 \pm 20 \ kJ \ mol^{-1}$. This value

220 was in agreement with the reported value by Lee et al. (2010) of $80 \ kJ \ mol^{-1}$ for the FAME-08

221 campaign. The estimated accommodation coefficient was 0.27, ranging from 0.1 to 0.8. This value

222 was a little higher than the 0.05 value reported in the earlier study. However, both suggest only

223 moderate resistances to mass transfer during the evaporation in the TD.

224   The corresponding measured and predicted thermograms are depicted in Figure 3. Almost

225 30% of the OA had not evaporated even after heating at 400 °C. The temperature at which half of

226 the OA evaporated was T_{50}=120 °C, a value similar to that observed by Lee et al. (2010). The

227 composition of the OA leaving the TD changed significantly as temperature increased according

228 to the model. At 125 °C the LVOCs and ELVOCs contributed equally to the remaining OA mass.

229 For further temperature increases the LVOC fraction was reduced until 375 °C, at which point only

230 the ELVOCs remained.

231   PMF analysis resulted in a two-factor solution (Florou et al., in prep.). Factor 1

232 corresponded to more oxidized oxygenated OA (MO-OOA) and Factor 2 to a less oxidized

233 component (LO-OOA). The average contribution of the two factors was 47% for the MO-OOA

234 and 53% for the LO-OOA. The O:C for the MO-OOA was 0.95 ($OS_C = 0.59$) and for the LO-

235 OOA it was 0.56 ($OS_C = -0.27$). The Finokalia area is characterized by the absence of local sources

236 and as result the absence of fresh OA. The OA during FAME-08, was also found to consist entirely

237 of OOA with no primary OA present (Hildebrandt et al., 2010). POA evaporates and gets oxidized

238 rapidly in the photochemically active environment of the Eastern Mediterranean during its

239 transport from its sources to this remote site.

240   The volatility distributions of the two PMF factors were estimated following the same

241 approach as that for the total OA. The measured thermograms for the two PMF factors are shown

242 in Figure 4. Almost 50% of both the MO-OOA and the LO-OOA evaporated at 150 °C. Almost

243 30% of the MO-OOA mass, and about 20% of the LO-OOA did not evaporate even at temperatures

244 as high as 400°C. The model reproduced the observed MFR values for both factors. Both factors

245 contained components with a wide volatility range. The MO-OOA exhibited a bimodal volatility

246 distribution with peaks at effective saturation concentrations of 10^{-8} and $10 \ \mu g \ m^{-3}$. Its effective

247 enthalpy of vaporization was approximately $90 \pm 35 \ kJ \ mol^{-1}$ and its accommodation coefficient

248 was 0.27. The estimated volatility distribution of the LO-OOA was a little more uniform peaking

249 at an effective saturation concentration of 1 $\mu g\ m^{-3}$. The calculated average volatility of LO-OOA

250 was 0.016 $\mu g\ m^{-3}$, an order of magnitude higher than that of the MO-OOA. The LO-OOA enthalpy

251 of vaporization was 70 ± 20 kJ mol^{-1}, 20 kJ mol^{-1} lower than that of the MO-OOA. Its

252 accommodation coefficient was approximately 0.1 indicating small mass transfer resistances. MO-

253 OOA consisted of approximately 40% SVOCs, 30% LVOCs, and 30% ELVOCs. On the contrary,

254 LO-OOA consisted of almost 45% SVOCs, 40% LVOCs and only 15% ELVOCs.

255   The fitting of the individual factor thermograms implicitly assumes that each factor had the

256 same size distribution as the total OA and also that the two factors were externally mixed. The

257 uncertainty introduced by these two assumptions was implicitly evaluated comparing the estimated

258 total OA of volatility distribution with the composition-weighted average of the volatility

259 distributions of the two OA factors. The two distributions agreed within a few percent for $10^{-3} < C^* <$

260 10^0 and within 10% for the lowest and highest volatility bins.

261

262 **4.2 Aerosol optical properties**

263   The measured b_{scat} at 405 nm ranged from 11.5 to 47 Mm^{-1} with an average campaign value

264 of 26.5 Mm^{-1} (Figure 5). Similarly, b_{abs} at 405 nm ranged from 0.64 to 5.6 Mm^{-1} with an average

265 value of 2.1 Mm^{-1}.

266   Acetonitrile is a known biomass burning marker and can help identify the potential

267 influence of the site by biomass burning events or wildfires during the campaign. The acetonitrile

268 concentration measured by the PTR-MS remained close to 0.4 ppb during the campaign, which is

269 the local background level. This together with the low BC levels indicate that the site was not

270 impacted by nearby biomass burning during the study.

271   The $b_{abs,405}$ variation followed that of the rBC ($R^2=0.74$ for the hourly averages). The ratio

272 of the $b_{abs,405}$ over the rBC, MAC_{405}, was equal to 16.3 ± 4.2 $m^2\ g^{-1}$. Previous studies have shown

273 that freshly generated BC has a MAC_{532} of 7.5 $m^2\ g^{-1}$ (Clarke et al., 2004; Bond and

274 Bergstrom, 2006). Using the definition of the AAE,

275 $$AAE = -\frac{\ln\left[MAC_{405}/MAC_{532}\right]}{\ln\left[405/532\right]},$$

276 we can calculate the MAC of freshly generated BC 405 nm. Assuming that the AAE is equal to

277 unity for BC particles, we find that the MAC_{405} of BC was approximately 9.9 $m^2\ g^{-1}$. The difference

278   between the measured and the theoretical value of MAC$_{405}$ can be due to the coating of BC by

279   other PM components (lensing effect) and/or the existence of other absorbing material. This will

280   be explored below.

281   The campaign average AAE of PM for wavelengths ranging from 370 to 950 nm was

282   0.97±0.22. The AAE of coated BC cores can deviate from the typical AAE=1 with values greater

283   or lower than unity (Gyawali et al., 2009). In addition, Lack and Cappa (2010) suggested that an

284   AAE>1.6 should confirm the presence of non-BC absorbing material, however an AAE<1.6 does

285   not exclude its presence.

286   Mie theory calculations were performed in order to estimate the MAC$_{405}$ and the E_{abs} due

287   to the lensing effect of the shell covering the BC core. Initially, a non-absorbing shell was assumed.

288   The predicted MAC$_{405}$ had an average value of 14.1 m^2 g^{-1}. The average E_{abs} due to lensing effect

289   was 2.07. The average predicted MAC$_{405}$ was 13% lower than the measured suggesting the

290   existence of non-refractory absorbing material (Figure 6).

291   In the next step, the Mie theory calculations were repeated assuming an absorbing shell

292   with a refractive index of n$_{OA}$ = 1.55 + ki, where the imaginary part, k, was allowed to vary from

293   0 to 0.4. This range of k values was selected based on previous literature (Kirchstetter et al., 2004;

294   Alexander et al., 2008; Chakrabarty et al., 2010; Chen and Bond, 2010; Saleh et al., 2014;

295   Chakrabarty et al., 2016, Li et al., 2016; Saleh et al., 2018). One third of the resulting k values

296   during the campaign were zero, suggesting a non-absorbing shell, while the other two thirds were

297   positive. More specifically, 22% of the estimated k values ranged from 0.01 to 0.1, 22% from 0.11

298   to 0.2, 19% from 0.21 to 0.3, and 4% of the k values ranged from 0.31 to 0.4.

299

300   **4.3 The role of ELVOCs**

301   The hypothesis that the presence of ELVOCs could explain the higher aerosol light

302   absorption was tested. The unexplained MAC (ΔMAC) difference of measured and predicted

303   values was compared with the total ELVOC mass concentration. The ELVOC concentration was

304   estimated based on the results on the volatility analysis of the two PMF factors:

305   [ELVOC]= 0.15 [LO-OOA] + 0.3 [MO-OOA]

306   The least-squares fit between the 3-hour averaged ΔMAC and ELVOC had R^2=0.65 (Figure 7).

307   This result suggests that the ELVOCs were probably contributing to the total absorption and could

308   explain the difference in the MAC.

5. Conclusions

A month-long campaign was conducted at a remote site, in Finokalia, Crete during May of 2016. The dominant PM_1 components were sulfate and aged organics with O/C=0.81. The average ambient OA concentration was 1.5 µg m^{-3} and the rBC was 0.14 µg m^{-3}. Continuous monitoring of biomass burning markers revealed that there was no detectable impact of wildfires on the site during the campaign. PMF analysis resulted in two secondary OA factors: one more oxidized (MO-OOA) and one less oxidized (LO-OOA). Total OA consisted on average of 40% SVOCs, 35% LVOCs and 25% ELVOCs. Both OA components with a wide range of volatilities. Approximately 30% of the MO-OOA was ELVOCs, 30% LVOCs and 40% semi-volatile material. The LO-OOA was more volatile on average with 40% consisting of LVOCs and 45% of SVOCs and 15% of ELVOCs.

Aerosol optical properties were measured. The average b_{scat} at 405 nm was 26.5 Mm^{-1} and the average b_{abs} at 405 nm was 2.1 Mm^{-1}. Furthermore, the average AAE was 0.97 and the MAC_{405} was 16.3. Mie theory calculations were able to reproduce one third of the measured MAC_{405} values assuming core-shell morphology and a non-absorbing shell (k=0). We estimated that the non-absorbing shell was causing an enhancement of the absorption by a factor of 2.07. For the other two thirds of the measurements the presence of an absorbing shell with an average k of 0.21 was needed to explain the measurements.

The ELVOCs mass concentration was estimated using the volatility distributions of the two factors. The ELVOC concentration was highly correlated (R^2=0.65) with the difference of the unexplained MAC_{405}, defined as the difference of the measured MAC_{405} the measured and the one predicted by Mie theory for k=0.

Data availability. The data in the study are available from the authors upon request (spyros@chemeng.upatras.gr).

Author contributions. AT conducted the absorption measurements, analysed the results and wrote the paper. EL performed the thermodenuder measurements and analysed the results. KF performed the AMS measurements and analysed the results. AL performed the PTR-MS measurements and analysis. EK was responsible for the OA volatility analysis. CK coordinated the field campaign and assisted with all measurements. NW assisted with all measurements SNP was responsible for

the design and coordination of the study and the synthesis of the results. All co-authors contributed to the writing of the manuscript.

Competing interests. The authors declare that they have no conflict of interest.

Acknowledgements

This work was supported by U.S. Environmental Protection Agency STAR program [grant number R835035]. Travel support was provided by the European Research Infrastructure ACTRIS. The authors would like to thank the Finokalia station personnel for the accommodation and for providing the aethalometer measurements.

References

Alexander, D. T. L., Crozier, P. A., and Anderson, J. R.: Brown carbon spheres in East Asian outflow and their optical properties, Science, 321, 833–836, 2008.

An, W. J., Pathak, R. K., Lee, B. H., and Pandis, S. N.: Aerosol volatility measurement using an improved thermodenuder: Application to secondary organic aerosol, J. Aerosol Sci., 38, 305–314, 2007.

Andreae, M. O., and Gelencser, A.: Black carbon or brown carbon? The nature of light-absorbing carbonaceous aerosols, Atmos. Chem. Phys., 6, 3131–3148, 2006.

Bond, T. C., and Bergstrom, R. W.: Light absorption by carbonaceous particles: An investigative review, Aerosol Sci. and Technol., 40, 27–67, 2006.

Bond, T. C., Habib, G., and Bergstrom, R. W.: Limitations in the enhancement of visible light absorption due to mixing state, J. Geophys. Res., 111, D20211, 2006.

Bohren, C. F., and Huffman, D. R.: Absorption and scattering of light by small particles. Research supported by the University of Arizona and Institute of Occupational and Environmental Health, New York: Wiley Interscience, 1983.

Bougiatioti, A., Stavroulas, I., Kostenidou, E., Zarmpas, P., Theodosi, C., Kouvarakis, G., Canonaco, F., Prévôt, A. S. H., Nenes, A., Pandis, S. N., and Mihalopoulos, N.: Processing of biomass burning aerosol in the eastern Mediterranean during summertime, Atmos. Chem. Phys., 14, 4793–4807, 2014.

Canagaratna, M. R., Jimenez, J. L., Kroll, J. H., Chen, Q., Kessler, S. H., Massoli, P., Hildebrandt Ruiz, L., Fortner, E.,Williams, L. R., Wilson, K. R., Surratt, J. D., Donahue, N. M., Jayne, J. T., and Worsnop, D. R.: Elemental ratio measurements of organic compounds using aerosol mass spectrometry: characterization, improved calibration, and implications, Atmos. Chem. Phys., 15, 253–272, 2015.

Cappa, C. D., Zhang, X., Russell, L. M., Collier, S., Lee, A. K. Y., Chen, C.-L., Betha, R., Chen, S., Liu, J., Price, D. J., Sanchez, K. J., McMeeking, G. R., Williams, L. R., Onasch, T. B., Worsnop, D. R., Abbatt, J. and Zhang, Q.: Light Absorption by Ambient Black and Brown Carbon and its Dependence on Black Carbon Coating State for Two California, USA, Cities in Winter and Summer, J. Geophys. Res.,124, 1550−1577, 2019.

379   Cappa, C. D., Onasch, T. B., Massoli, P., Worsnop, D. R., Bates, T. S., Cross, E. S., Davidovits,
380   P., Hakala, J., Hayden, K. L., Jobson, B. T., Kolesar, K. R., Lack, D. A., Lerner, B. M., Li,
381   S. M., Mellon, D., Nuaaman, I., Olfert, J. S., Petäjä, T., Quinn, P. K., Song, C., Subramanian,
382   R., Williams, E. J., and Zaveri, R. A.: Radiative absorption enhancements due to the mixing
383   state of atmospheric black carbon, Science, 337, 2012.
384   Chakrabarty, R. K., Moosmuller, H., Chen, L.-W. A., Lewis, K., Arnott, W. P., Mazzoleni, C.,
385   Dubey, M. K., Wold, C. E., Hao, W. M., and Kreidenweis, S. M.: Brown carbon in tar balls
386   from smoldering biomass combustion, Atmos. Chem. Phys., 10,6363–6370, 2010.
387   Chakrabarty, R. K., Gyawali, M., Yatavelli, R. L. N., Pandey, A., Watts, A. C., Knue, J., Chen,
388   L.-W. A., Pattison, R. R., Tsibart, A., Samburova, V., and Moosmüller, H.: Brown carbon
389   aerosols from burning of boreal peatlands: microphysical properties, emission factors, and
390   implications for direct radiative forcing, Atmos. Chem. Phys., 16, 3033–3040, 2016.
391   Chen, Y. and Bond, T. C.: Light absorption by organic carbon from wood combustion, Atmos.
392   Chem. Phys., 10, 1773–1787, 2010.
393   Clarke, A. D., Shinozuka, Y., Kapustin, V. N., Howell, S., Huebert, B., Doherty, S., Anderson, T.,
394   Covert, D., Anderson, J., Hua, X., Moore, K. G., McNaughton, C., Carmichael, G., and
395   Weber, R.: Size distributions and mixtures of dust and black carbon aerosol in Asian outflow:
396   Physiochemistry and optical properties, J. Geophys. Res., 109, D15S09, doi.org/10.1029/
397   2003JD004378, 2004.
398   Donahue, N. M., Robinson, A. L., Stanier, C. O., and Pandis, S. N.: Coupled partitioning, dilution,
399   and chemical aging of semivolatile organics, Environ. Sci. Technol., 40, 2635–2643, 2006.
400   Florou, K., Liangou, A., Louvaris, E., Kaltsonoudis, C., Tasoglou, A., Patoulias, D., Kouvarakis,
401   G., Vlachou, A., Kourtchev, I. and Spyros N. Pandis, S. N.; The Finokalia Aerosol
402   Measurement Experiment (FAME-16): Atmospheric processing of organic aerosol in the
403   Eastern Mediterranean, in prep.
404   Fuller, K. A., Malm, W. C., and Kreidenweis, S. M.: Effects of mixing on extinction by
405   carbonaceous particles, J. Geophys. Res., 104, 15941–15954, 1999.
406   Gyawali, M., Arnott, W. P., Lewis, K., and Moosmueller, H.: In situ aerosol optics in Reno, NV,
407   USA during and after the summer 2008 California wildfires and the influence of absorbing
408   and non-absorbing organic oatings on spectral light absorption, Atmos. Chem. Phys., 9,
409   8007–8017, 2009.
410   Gysel, M., Laborde, M., Olfert, J. S., Subramanian, R., and Gröhn, A. J.: Effective density of
411   Aquadag and fullerene soot black carbon reference materials used for SP2 calibration,
412   Atmos. Meas. Tech., 4, 2851–2858, 2011.
413   Healy, R. M., Wang, J. M., Jeong, C.-H., Lee, A. K. Y., Willis, M. D., Jaroudi, E., Zimmerman,
414   N., Hilker, N., Murphy, M., Eckhardt, S., Stohl, A., Abbatt, J. P. D., Wenger, J. C., and
415   Evans, G. J.: Light-absorbing properties of ambient black carbon and brown carbon from
416   fossil fuel and biomass burning sources, J. Geophys. Res., 120, 6619–6633, 2015.
417   Hildebrandt, L., Engelhart, G. J., Mohr, C., Kostenidou, E., Lanz, V. A., Bougiatioti, A., DeCarlo,
418   P. F., Prévôt, A. S. H., Baltensperger, U., Mihalopoulos, N., Donahue, N. M., and Pandis, S.
419   N.: Aged organic aerosol in the eastern Mediterranean: The Finokalia aerosol measurement
420   experiment 2008, Atmos. Chem. Phys., 10, 4167–4186, 2010.
421   Hildebrandt, L., Kostenidou, E., Lanz, V. A., Prévôt, A. S. H., Baltensperger, U., Mihalopoulos,
422   N., Laaksonen, A., Donahue, N. M., and Pandis, S. N.: Sources and atmospheric processing
423   of organic aerosol in the Mediterranean: Insights from aerosol mass spectrometer factor
424   analysis, Atmos. Chem. Phys., 11, 12499–12515, 2011.

Jacobson, M. Z.: Strong radiative heating due to the mixing state of black carbon in atmospheric aerosols, Nature, 409, 695–697, 2001.

Kalivitis, N., Bougiatioti, A., Kouvarakis, G., and Mihalopoulos, N.: Long term measurements of atmospheric aerosol optical properties in the Eastern Mediterranean, Atmos. Res., 102, 351–357, 2011.

Karnezi, E., Riipinen, I., and Pandis, S. N.: Measuring the atmospheric organic aerosol volatility distribution: a theoretical analysis, Atmos. Meas. Tech., 7, 2953–2965, doi:10.5194/amt7-2953-2014, 2014.

Kirchstetter, T., Novakov, T., and Hobbs, P.: Evidence that the spectral dependence of light absorption by aerosols is affected by organic carbon, J. Geophys. Res., 109, D21208, doi.org/10.1029/2004JD004999, 2004.

Kirchstetter, T. W., and Novakov, T.: Controlled generation of black carbon particles from a diffusion flame and applications in evaluating black carbon measurement methods, Atmos. Environ., 41, 1874–1888, 2007.

Knox, A., Evans, G. J., Brook, J. R., Yao, X., Jeong, C.-H., Godri, K. J., Sabaliauskas, K., and Slowik, J. G.: Mass absorption cross-section of ambient black carbon aerosol in relation to chemical age, Aerosol Sci. Tech., 43, 522-532, 2009.

Kostenidou, E., Pathak, R. K., and Pandis, S. N.: An algorithm for the calculation of secondary organic aerosol density combining AMS and SMPS data, Aerosol Sci. Tech., 41, 1002–1010, 2007.

Kouvarakis, G., Tsigaridis, K., Kanakidou, M., and Mihalopoulos, N.: Temporal variations of surface regional background ozone over Crete Island in the Southeast Mediterranean, J. Geophys. Res., 105, 399–407, 2000.

Lack, D. A., Langridge, J. M., Bahreini, R., Cappa, C. D., Middlebrook, A. N., and Schwarz, J. P.: Brown carbon and internal mixing in biomass burning particles, Proc. Natl. Acad. Sci. USA, 109, 14802–14807, 2012.

Lack, D. A., and Cappa, C. D.: Impact of brown and clear carbon on light absorption enhancement, single scatter albedo and absorption wavelength dependence of black carbon, Atmos. Chem. Phys., 10, 4207–4220, 2010.

Lanz, V. A., Alfarra, M. R., Baltensperger, U., Buchmann, B., Hueglin, C., and Prévôt, A. S. H.: Source apportionment of submicron organic aerosols at an urban site by factor analytical modelling of aerosol mass spectra, Atmos. Chem. Phys., 7, 1503–1522, 2007.

Lee, B. H., Kostenidou, E., Hildebrandt, L., Riipinen, I., Engelhart, G. J., Mohr, C., Decarlo, P. F., Mihalopoulos, N., Prévôt, A. S. H., Baltensperger, U., and Pandis, S. N.: Measurement of the ambient organic aerosol volatility distribution: Application during the Finokalia Aerosol Measurement Experiment (FAME-2008), Atmos. Chem. Phys., 10, 12149–12160, 2010.

Lelieveld, J., Berresheim, H., Borrmann, S., Crutzen, P. J., Dentener, F. J., Fischer, H., Feichter, J., Flatau, P. J., Heland, J., Holzinger, R., Korrmann, R., Lawrence, M. G., Levin, Z., Markowicz, K. M., Mihalopoulos, N., Minikin, A., Ramanathan, V., de Reus, M., Roelofs, G. J., Scheeren, H. A., Sciare, J., Schlager, H., Schultz, M., Siegmund, P., Steil, B., Stephanou, E. G., Stier, P., Traub, M., Warneke, C., Williams, J., and Ziereis, H.: Global air pollution crossroads over the mediterranean, Science, 298, 794–799, 2002.

Li, X., Chen, Y., and Bond, T. C.: Light absorption of organic aerosol from pyrolysis of corn stalk, Atmos. Environ. 144, 249–256, 2016.

Liu, D., Whitehead, J., Alfarra, M. R., Reyes-Villegas, E., Spracklen, D. V., Reddington, C. L., Kong, S., Williams, P. I., Ting, Y.-C., Haslett, S., Taylor, J. W., Flynn, M. J., Morgan, W.

471   T., McFiggans, G., Coe, H., and Allan, J. D.: Black-carbon absorption enhancement in the
472   atmosphere determined by particle mixing state, Nat. Geosci., 10, 184–188, 2017.
473 Liu, S., Aiken, A. C., Gorkowski, K., Dubey, M. K., Cappa, C. D., Williams, L. R., Herndon, S.
474   C., Massoli, P., Fortner, E. C., Chhabra, P. S., Brooks, W. A., Onasch, T. B., Jayne J. T.,
475   Worsnop, D. R., China, S., Sharma, N., Mazzoleni, C., Xu, L., Ng, N. L., Liu, D., Allan, J.
476   D., Lee, J. D., Fleming, Z. L., Mohr, C., Zotter, P., Szidat, S., and Prévôt, A. S. H.: Enhanced
477   light absorption by mixed source black and brown carbon particles in UK winter, Nat
478   Commun., 6, 843, 2015.
479 Louvaris, E. E., Florou, K., Karnezi, E., Papanastasiou, D. K., Gkatzelis, G. I., and Pandis, S. N.:
480   Volatility of source apportioned wintertime organic aerosol in the city of Athens, Atmos.
481   Environ., 158, 138-147, 2017.
482 McMeeking, G. R., Fortner, E., Onasch, T. B., Taylor, J. W., Flynn, M., Coe, H., and Kreidenweis,
483   S. M.: Impacts of nonrefractory material on light absorption by aerosols emitted from
484   biomass burning, J. Geophys. Res., 119, 12272–12286, 2014.
485 Mihalopoulos, N., Stephanou, E., Kanakidou, M., Pilitsidis, S., and Bousquet, P.: Tropospheric
486   aerosol ionic composition in the eastern Mediterranean region, Tellus, 49B, 314–326, 1997.
487 Mullins, J., and Williams, A.: The optical properties of soot: A comparison between experimental
488   and theoretical values, Fuel, 66, 277–280, 1987.
489 Paatero, P., and Tapper, U.: Positive matrix factorization: A non-negative factor model with
490   optimal utilization of error estimates of data values, Environmetrics, 5, 111–126, 1994.
491 Park, K., Kittelson, D. B., Zachariah, M. R., and McMurry, P. H.: Measurement of inherent
492   material density of nanoparticle agglomerates, J. Nanopart. Res., 6, 267–272, 2004.
493 Pikridas, M., Bougiatioti, A., Hildebrandt, L., Engelhart, G. J., Kostenidou, E., Mohr, C., Prevót,
494   A. S. H., Kouvarakis, G., Zarmpas, P., Burkhart, J. F., Lee, B.-H., Psichoudaki, M.,
495   Mihalopoulos, N., Pilinis, C., Stohl, A., Baltensperger, U., Kulmala, M., and Pandis, S. N.:
496   The Finokalia Aerosol Measurement Experiment – 2008 (FAME-08): an overview, Atmos.
497   Chem. Phys., 10, 6793–6806, 2010.
498 Riipinen, I., Pierce, J. R., Donahue, N. M., and Pandis, S. N.: Equilibration time scales of organic
499   aerosol inside thermodenuders: Kinetics versus equilibrium thermodynamics, Atmos.
500   Environ., 44, 597–607, 2010.
501 Saleh, R., Cheng, Z., and Atwi., K.: The brown–black continuum of light-absorbing combustion
502   aerosols, Environ. Sci. Technol. Lett. 5, 508–13, 2018.
503 Saleh, R., Robinson, E. S., Tkacik, D. S., Ahern, A. T., Liu, S., Aiken, A. C., Sullivan, R. C.,
504   Presto, A. A., Dubey, M. K., Yokelson, R. J., Donahue, N. M., and Robinson, A. L.:
505   Brownness of organics in aerosols from biomass burning linked to their black carbon content,
506   Nat. Geosci., 7, 647–650, 2014.
507 Saliba, G., Subramanian, R., Saleh, R., Ahern, A. T., Lipsky, E. M., Tasoglou, A., Sullivan, R. C.,
508   Bhandari, J., Mazzoleni, C., and Robinson, A. L.: Optical properties of black carbon in
509   cookstove emissions coated with secondary organic aerosols: Measurements and modeling,
510   Aerosol Sci. Technol., 50, 1264–1276, 2016.
511 Tasoglou, A., Saliba, G., Subramanian, R., and S. N. Pandis S. N.: Absorption of chemically aged
512   biomass burning carbonaceous aerosol, J. Aerosol. Sci., 113, 141–52, 2017.
513 Ulbrich, I. M., Canagaratna, M. R., Zhang, Q., Worsnop, D. R., and Jimenez, J. L.: Interpretation
514   of organic components from Positive Matrix Factorization of aerosol mass spectrometric
515   data, Atmos. Chem. Phys., 9, 2891–2918, 2009.

516 Vrekoussis, M., Liakakou, E., Koçak, M., Kubilay, N., Oikonomou, K., Sciare, J., and
517   Mihalopoulos, N.: Seasonal variability of optical properties of aerosols in the eastern
518   Mediterranean, Atmos. Environ., 39, 7083-7094, 2005.
519 Weingartner, E., H. Saathoff, M. Schnaiter, N. Streit, B. Bitnar, and U. Baltensperger: Absorption
520   of light by soot particles: Determination of the absorption coefficient by means of
521   aethalometers, J. Aerosol. Sci. 34, 1445–63, 2003.
522 Wu, J.-S., Krishnan, S. S., and Feath, G. M.: Refractive indices at visible wavelengths of soot
523   emitted from buoyant turbulent diffusion flames, J. Heat Transfer, 119, 230–237, 1997.
524 Zanatta, M., Laj, P., Gysel, M., Baltensperger, U., Vratolis, S., Eleftheriadis, K., Kondo, Y.,
525   Dubuisson, P., Winiarek, V., Kazadzis, S., Tunved, P., and Jacobi, H. W.: Effects of mixing
526   state on optical and radiative properties of black carbon in the European Arctic, Atmos.
527   Chem. Phys., 18, 14037-14057, 2018.
528 Zhang, Y.; Favez, O.; Canonaco, F.; Liu, D.; Močnik, G.; Amodeo, T.; Sciare, J.; Prévôt, A. S. H.;
529   Gros, V., and Albinet, A.: Evidence of major secondary organic aerosol contribution to
530   lensing effect black carbon absorption enhancement, NPJ Climate and Atmospheric Science,
531   1, doi.org/10.1038/s41612-018-0056-2, 2018a.
532 Zhang, Y., Zhang, Q., Cheng, Y., Su, H., Li, H., Li, M., Zhang, X., Ding, A., and He, K.:
533   Amplification of light absorption of black carbon associated with air pollution, Atmos.
534   Chem. Phys., 18, 9879–9896, 2018b.
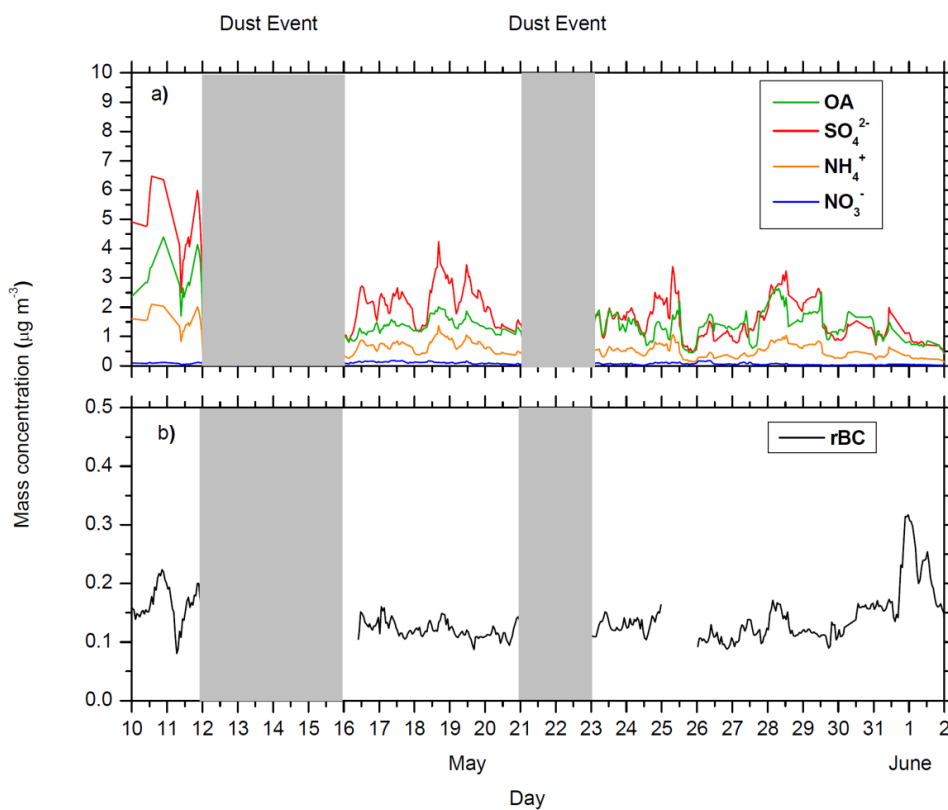
Figure 1: Evolution of the aerosol chemical composition based on the HR-TOF-AMS and SP2 measurements during FAME-16: a) the non-refractory aerosol components; b) rBC concentration. The shaded areas represent the dust events periods.
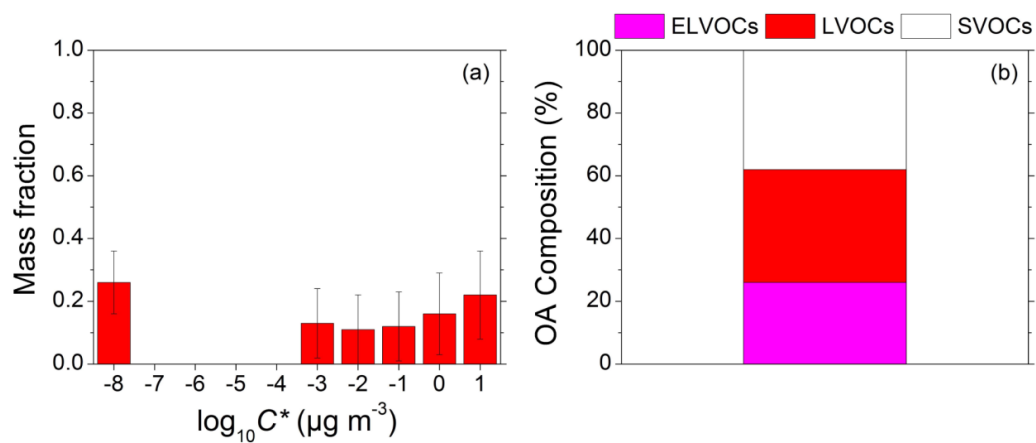
541

542   **Figure 2:** (a) Total OA volatility distribution along with its uncertainty estimated by the Karnezi

543   et al. (2014) approach. The error bars represent the corresponding variability (± 1 standard

544   deviation). (b) OA composition. Magenta color represents the ELVOCs, red the LVOCs, and white

545   the SVOCs.

546

547
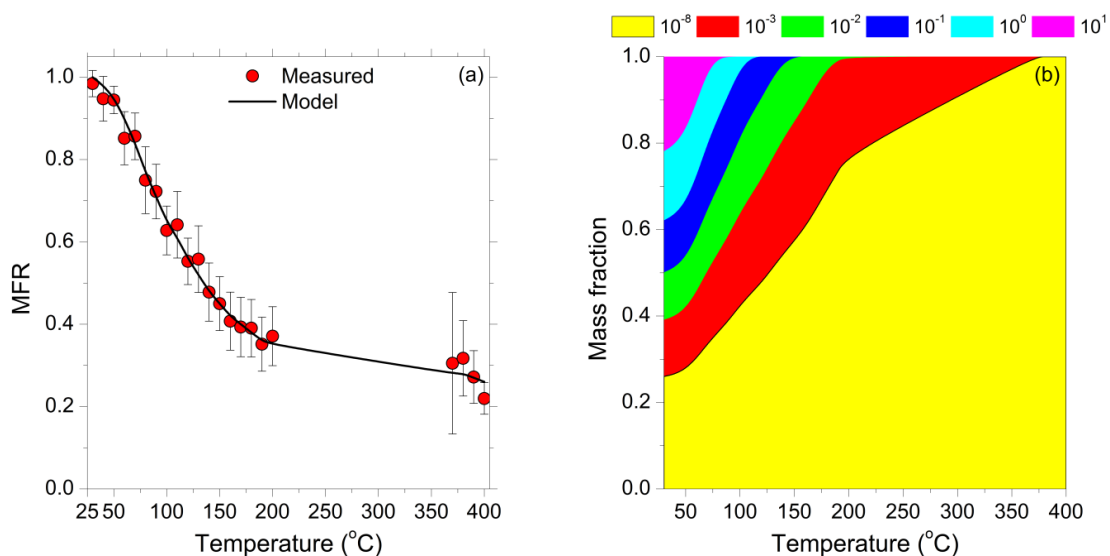
Figure 3: (a) Average loss-corrected total OA thermograms. Red circles represent the measured total OA MFR and the error bars the corresponding variability (± 2 standard deviations of the mean). The solid lines are the model predictions (b) Mass fraction of the total OA for different effective saturation surrogate species with concentrations as a function of TD temperature. Yellow color represents the contribution of the effective saturation concentration $C^* = 10^{-8}$ µg m^{-3}, red the contribution of the $C^* = 10^{-3}$ µg m^{-3}, green the $C^* = 10^{-2}$ µg m^{-3}, blue the $C^* = 10^{-1}$ µg m^{-3}, cyan the $C^* = 10^{0}$ µg m^{-3}, and magenta the $C^* = 10$ µg m^{-3}.

555

556
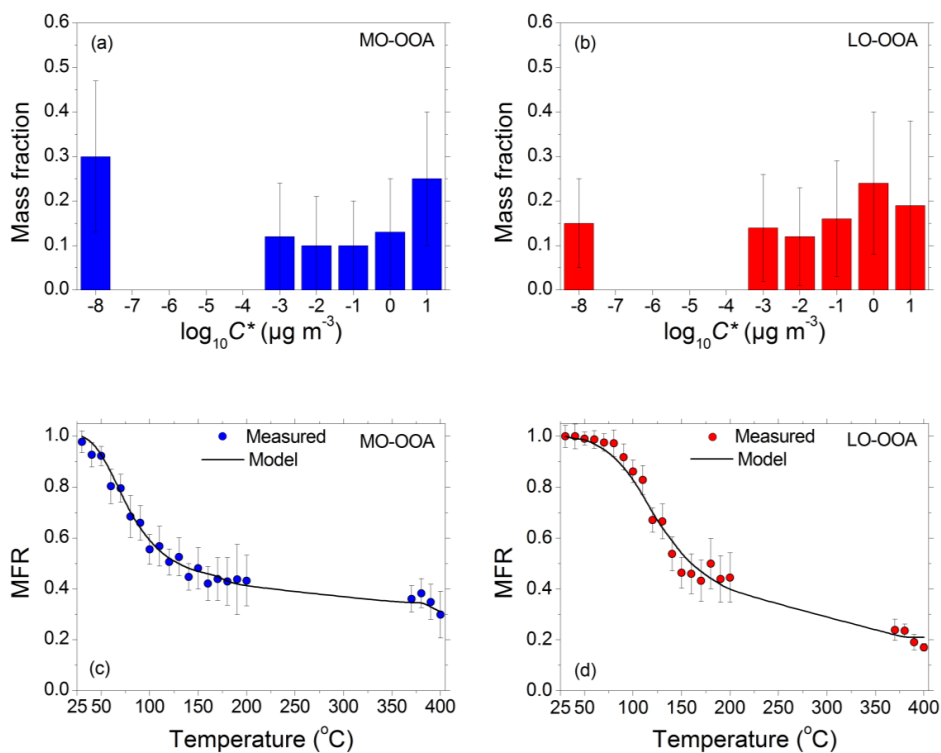
Figure 4: (a) Estimated volatility distribution of the MO-OOA factor along with its corresponding uncertainties by using the approach of Karnezi et al. (2014). (b) Estimated volatility distribution of the LO-OOA factor along with its corresponding uncertainties. (c) Measured (in circles) and predicted thermograms for the LO-OOA factor. The error bars represent ± 2 standard deviations of the mean. (d) Measured (in circles) and predicted thermograms for the LO-OOA factor. The error bars represent ± 2 standard deviations of the mean.

563

564
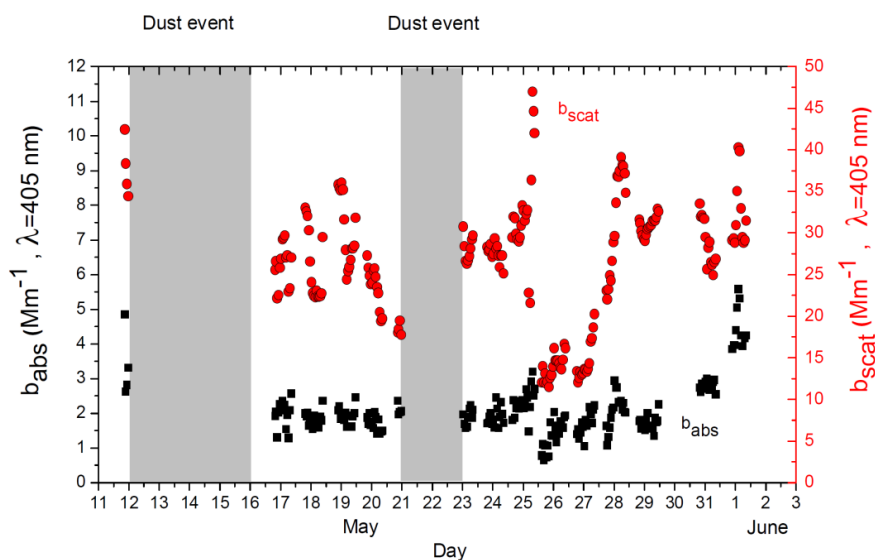
Figure 5: The timeseries of the aerosol optical properties at λ=405 nm. The black squares represent

the absorption coefficient, b_{abs}, while the red circles represent the scattering coefficient, b_{scat}. The

shaded areas represent the dust events periods.

568

569
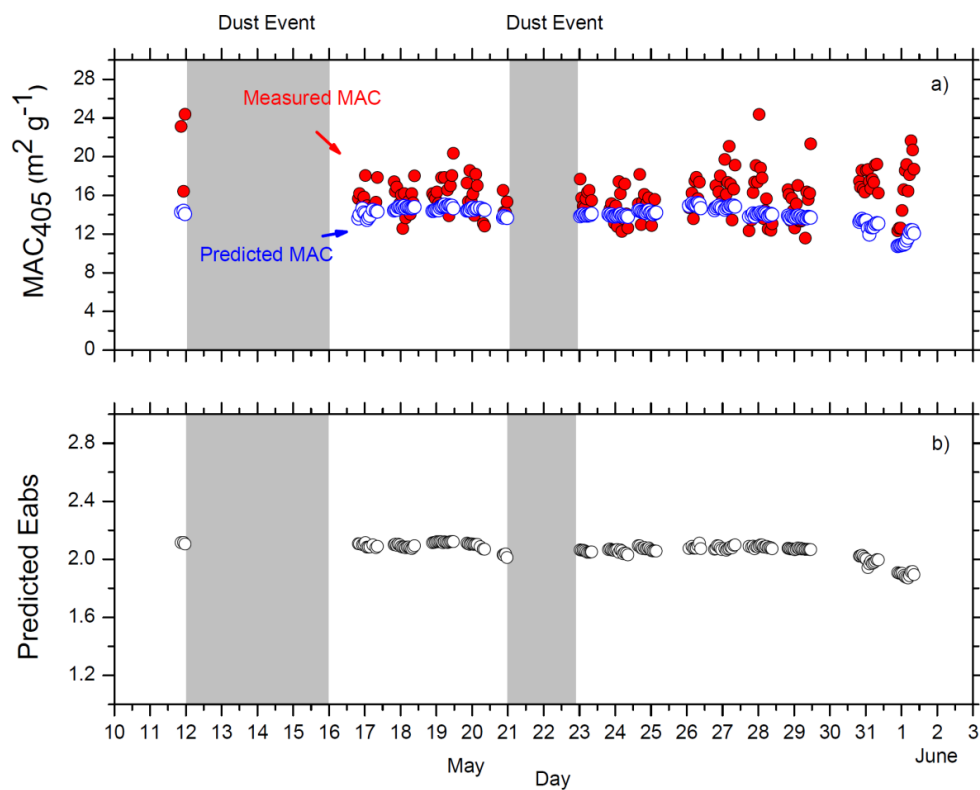
Figure 6: Results from the Mie theory calculations, assuming a non-absorbing shell (k=0): a) predicted (blue circles) and measured MAC_{405} (red circles). b) Predicted E_{abs} values. The shaded areas represent the dust events periods.

573

574
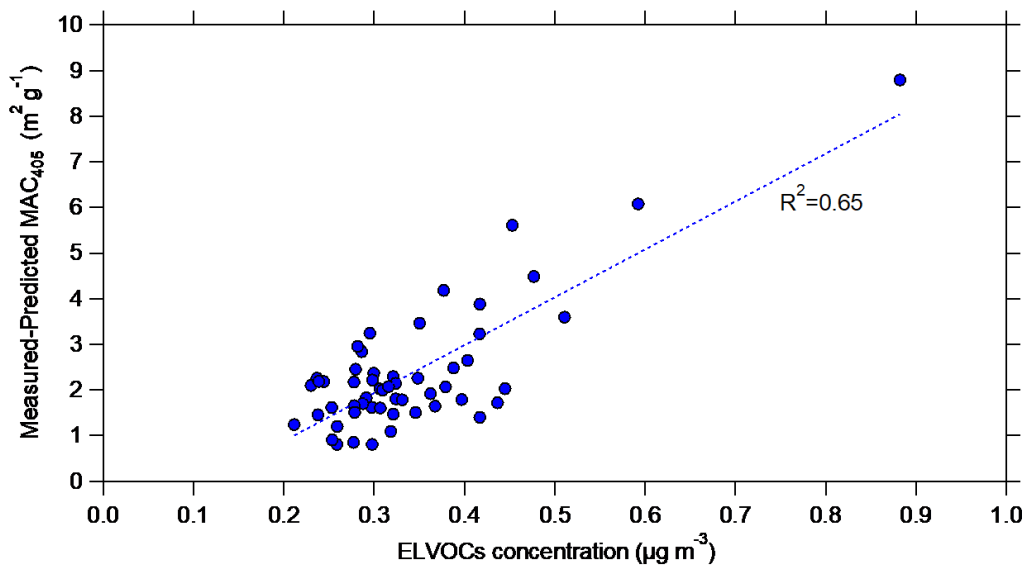
Figure 7: Difference between the measured and the predicted MAC_{405} as a function of the estimated concentration of the ELVOCs.

575

576

577